A contactless single-step process for simultaneous nanoscale patterning and cleaning of large-area graphene

2D Materials

PAPER

A contactless single-step process for simultaneous nanoscale patterning and cleaning of large-area graphene

Tuan T Tran[1,*], Henrik Bruce[1], Ngan Hoang Pham[2] and Daniel Primetzhofer[1]

[1] Department of Physics and Astronomy, Ångström Laboratory, Uppsala University, Box 516, SE-751 20 Uppsala, Sweden
[2] Division of Solid-State Electronics, Department of Electrical Engineering, Uppsala University, SE-751 03 Uppsala, Sweden
* Authors to whom any correspondence should be addressed.

E-mail: Tuan.Tran@physics.uu.se

Keywords: graphene, 2D materials, nanomesh, porous, patterning, cleaning, ion irradiation

Supplementary material for this article is available online

OPEN ACCESS

RECEIVED
6 December 2022

REVISED
17 February 2023

ACCEPTED FOR PUBLICATION
1 March 2023

PUBLISHED
9 March 2023

Abstract

The capability to structure two-dimensional materials (2DMs) at the nanoscale with customizable patterns and over large areas is critical for a number of emerging applications, from nanoelectronics to 2D photonic metasurfaces. However, current technologies, such as photo- and electron-beam lithography, often employing masking layers, can significantly contaminate the materials. Large-area chemical vapour deposition-grown graphene is known to have non-ideal properties already due to surface contamination resulting from the transferring process. Additional contamination through the lithographic process might thus reduce the performance of any device based on the structured graphene. Here, we demonstrate a contactless chemical-free approach for simultaneous patterning and cleaning of self-supporting graphene membranes in a single step. Using energetic ions passing through a suspended mask with pre-defined nanopatterns, we deterministically structure graphene with demonstrated feature size of 15 nm, approaching the performance of small-area focused ion beam techniques and extreme ultraviolet lithography. Our approach, however, requires only a broad beam, no nanoscale beam positioning and enables large area patterning of 2DMs. Simultaneously, in regions surrounding the exposed areas, contaminations commonly observed on as-grown graphene targets, are effectively removed. This cleaning mechanism is attributed to coupling of surface diffusion and sputtering effects of adsorbed surface contaminants. For applications using 2DMs, this simultaneous patterning and cleaning mechanism may become essential for preparing the nanostructured materials with improved cleanliness and hence, quality.

1. Introduction

Techniques to deterministically structure two-dimensional materials (2DMs), such as graphene, over large areas are highly sought after for a variety of applications, such as nanoelectronics [1–4], 2D photonic metasurfaces [5–7], and chemical filtering [8–11]. For electronic applications, structuring the graphene membranes into nanoscale, nanomeshes and nanoribbons can open up the Dirac cone of the material's band structure, essentially transforms it from a semimetal to a semiconductor with a bandgap sufficient for room temperature operation [1, 12–16]. Since graphene has excellent carrier mobility [17, 18], such structured graphene with a sizable band gap is expected to have a great impact on future applications. For photonic application, periodic structures with feature size smaller than the wavelengths of light, i.e. metasurfaces, can be used to control the polarization, phase and amplitude of light. Metasurfaces fabricated from 2DMs can minimize the size of the optical devices, reduce optical losses and the effect of dispersion, as compared to the bulk counterparts [5]. Nanostructured graphene, which has long-lived plasmons, has been demonstrated by simulation to be able to tune electrically the polarization of light with a performance several orders of magnitude higher than metal nanoparticles of similar size [6]. For filtering applications, perforated self-supporting graphene membranes have been shown to feature outstanding

efficiency and selectivity by both, calculations [9, 19] and experiments [10, 11, 20].

To realize patterned graphene, a number of experimental methods have been demonstrated. For high precision structuring over small areas, focused electron and ion beams can be employed [11, 21–24]. Using focused beams of Ga^+ and He^+ ions, Celebi *et al* have produced self-supporting graphene membranes with a few million pores having narrowly distributed sizes below 10 nm [11]. Although the focused beam approach provides high precision and pore size below 10 nm, it has limited scalability due to the stringent focusing requirements and small field of view (tens of micrometers). Nowadays, large-scale, even roll-to-roll, graphene membranes are commercially available [25], setting demands for a more scalable approach. Using ultraviolet (UV) oxidative etching, large-area nanoporous graphene can be produced with a large number of sub-nanometer pores, suitable for water desalination and filtering applications [10, 26]. Irradiation with highly charged low energy ions and swift heavy ions have also been demonstrated for perforating self-supporting graphene and molybdenum disulfide monolayers (MLs) [27–31]. However, for structuring graphene membranes with pre-defined patterns by oxidative or ion beam techniques pattern-defining layers are necessary. These are coated directly onto the graphene membrane. Examples of pattern-defining layers include self-assembly of polystyrene nanosphere [1, 2], block copolymers [32, 33], nanoimprinting [34, 35], atomic force microscopy (AFM) based nanolithography [36, 37], porous anodic alumina [15], electron beam lithography (EBL) [38], and extreme UV lithography [39]. The downsides of using coating layers are, at first, the fact that the approach introduces a significant amount of contamination which is difficult to be subsequently removed completely [40, 41], and second, the damage to the self-supporting membranes due to the chemical and the mechanical forces involved. Contamination on graphene is a serious issue as they significantly deteriorate the desired properties of the material [42, 43]. Large-area graphene grown by chemical vapor deposition is known to be contaminated already after being transferred from the growth substrates to other substrates [40, 44]. Adding additional contamination to the material due to the masking layers would thus make it worse, let aside inevitable damage to the graphene lattice upon attempted complete removal.

In this letter, a contactless and scalable approach to effectively structure large-area self-supporting graphene membrane with pre-defined patterns is demonstrated. The basic methodology is shown in figure 1(a), illustrating how a broad beam of energetic ions passes through a suspended silicon mask with the desired nanopatterns and structures the underlying graphene. Perforation of the graphene matrix is achieved through nuclear interactions between the primary ions and the carbon atoms, with the structure of the pattern determined by the structure of the mask. Simultaneously, during patterning, surface diffusion of contaminants and effective sputtering of physi- and chemisorbed species leads to an effective removal of contaminants even in unirradiated areas. The key component of the approach is a suspended silicon mask produced through a multi-step nanofabrication process, including in particular EBL. With an ultrafine electron probe, EBL provides unlimited capability in structural designs and excellent spatial resolution of a few nanometers. Although producing the mask is time consuming, it can be used repeatedly without losing the defined structures. Hence, the developed methodology represents a scalable approach. The use of a conventional well-established ion implanter for the irradiation gives us the capabilities of precisely controlling the necessary ion doses, ion species, and ion energies, which strongly affect the structuring process. As compared to electrons and photons, the rest mass of the ions is much higher, equivalent to an extremely short de Broglie wavelength, on the order of femtometers. Therefore, resolution-limiting effects due to diffraction through the nanopores are not to be expected. The beam is in general expected to travel along a straight trajectory, allowing for a certain gap between the mask and the samples, and hence enabling a contactless approach. Ion implantation is one of the most deterministic methods for modification of materials, in which the nuclear and electronic energy deposition, the temperature dependence, and the irradiation environments can be precisely controlled. Therefore, the combination of EBL-fabricated masks and ion implantation provides the best of two worlds: design flexibility, nanoscale resolution, and deterministic patterning.

2. Experiments

Figure 1(b) shows the cross-section of the suspended mask before the final back-side etching for releasing the membrane. The top layer of the membrane is 60 nm Au/Cr for discharging purposes during the irradiation. The second layer comprises of 340 nm Si(100) providing the mechanical strength of the membrane. The dimension of the membrane is about 1×1 mm^2 on which several different patterns were created. Each pattern features 150×150 pores having different diameters and identical pitch of 500 nm. While we show here only pores with circular shape with certain sizes and arrangements, there is no limitation on the structural design of the patterns. The bottom layer is formed by 150 nm SiO_2 on a Si(100) substrate which are both removed later using deep reactive ion etching and wet hydrofluoric acid etching. Details on the mask fabrication process are provided in the supplementary section. Figures 1(c)–(f) show the backside of the final membrane with

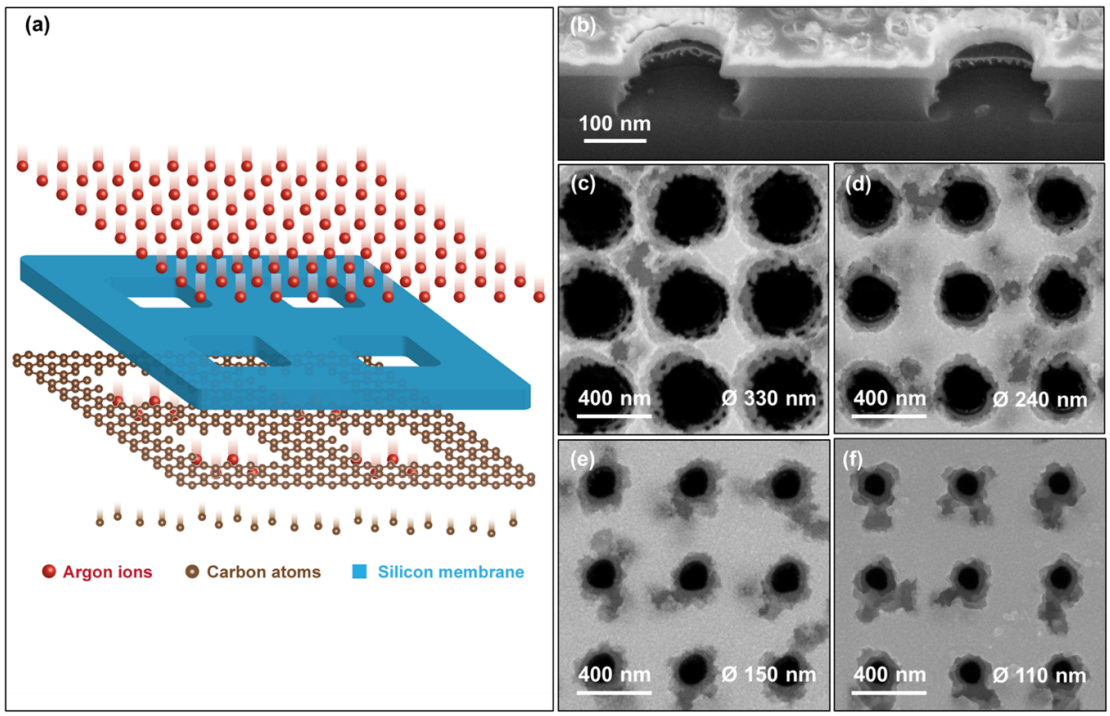

Figure 1. Illustration of the structuring approach: a broad and uniform beam of ions with keV kinetic energy passes through a suspended nanopatterned mask and induces a pre-defined pattern on graphene (a). Cross-sectional SEM image of the mask before back-side etching showing the individual layers of the membrane: the top layer is 60 nm Au/Cr to prevent charging during the ion irradiation, next is the 340 nm Si (100) layer followed by a SiO_2 layer on a Si (100) substrate (b). SEM images of the masks after back-side etching as seen from the back exhibiting through-hole patterns of different sizes, from 110 nm to 330 nm (c)–(f).

the through-hole pore patterns. The diameter of the pores ranges from 110 nm to 330 nm. The ion irradiation was done with a 20 keV Ar^+ beam at a dose of 1×10^{16} At cm^{-2} at room temperature. The vacuum level inside the irradiation chamber is in the order of 10^{-6} mbar. The ion energy of 20 keV was chosen to maximize nuclear interactions and hence obtain effective sputtering, while maintaining excellent beam properties such as minimum divergence. At this energy, a considerable amount of the ion energy is furthermore transferred through electronic interactions, leading to desirable cleaning effects as will be shown later. The whole structuring process has only one step, much simpler than the multi-step processes of conventional lithographic techniques. In addition, this approach is particularly suitable for structuring self-supporting 2D membranes as no chemical and mechanical processing is required, which might negatively affect the membranes.

The samples are self-supporting ML graphene on QUANTIFOIL® transmission electron microscopy (TEM) Cu grid, which is commercially available from Graphenea. Since graphene and the TEM grid made of Cu are both very conductive, charging effect does not usually occur in the sample during and after ion irradiation. The QUANTIFOIL® R2/4 used for these samples has periodical holes of about 2 μm with a distance of 4 μm between the holes. The areas within the 2 μm holes are self-supporting ML graphene as shown in figure 2. The graphene was grown using chemical vapor deposition on Cu substrates and then transferred onto the QUANTIFOIL® TEM grid using a wet transfer process. It is this transfer process that usually leaves large amount of polymethyl methacrylate (PMMA) contamination on the graphene, significantly deteriorating the graphene's properties [40, 44]. Removing the PMMA contaminants from graphene is still a serious issue which has been addressed by many studies. In these, a number of different methods have been demonstrated with different degrees of success, including thermal annealing, plasma treatment, ion beam, mechanical, and light treatment. However, satisfactory cleaning results do not seem to be achieved yet as most methods while to some extent reducing the level of contamination also induce permanent structural damages to the graphene lattice. Comprehensive reviews on the topic are available, such as in [44, 45]. In a separate supplementary section, we provide additional details of the experiments as well as other results.

3. Results

Figure 2 shows the scanning electron microscopy (SEM) images of the graphene membranes after ion irradiation. All presented results are taken from one sample after one irradiation so that a more conclusive comparison can be made. The membranes presented in figures 2(a)–(c) feature almost identical circular pore structures as the mask in figures 1(c)–(e)

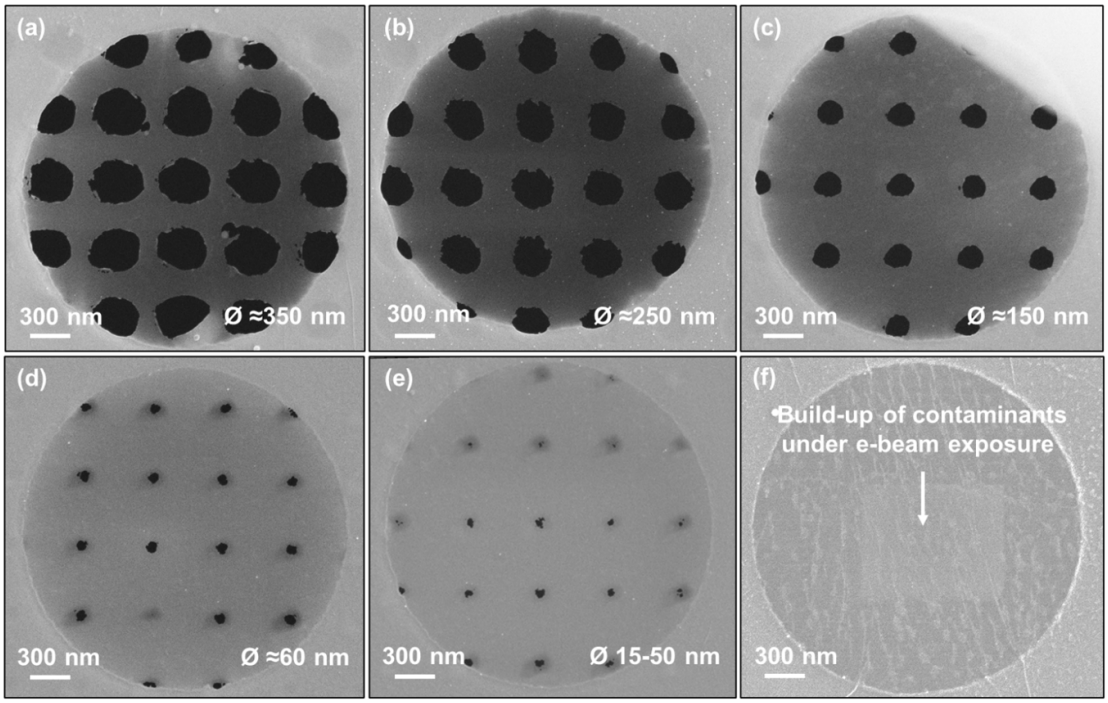

Figure 2. SEM images of the self-supporting graphene membrane within ∼2 μm circular openings of the QUANTIFOIL® support after being structured with a 20 keV Ar^+ beam at a dose of 1×10^{16} At cm^{-2}. For the first three images (a)–(c), the structures of the graphene are closely resemblant to those of the mask shown in figures 1(c)–(e). Smaller structures, from 60 nm (d) down to 15 nm (e) can also be found in areas in proximity to the border of the 110 nm pattern. (f) SEM image of the unirradiated graphene area showing apparent streaks of the PMMA contaminants.

with pore diameter ranging from 150 nm to 350 nm, demonstrating the ability of the method in transferring the structure of the mask to the graphene. For the 110 nm pattern, in particular at areas close to the border of the pattern, pores with diameter much smaller than 110 nm have been found, such as 60 nm (figure 2(d)), and 15–50 nm (figure 2(e)). As being addressed later, these smaller pores are caused by the diffusion of excess contamination from the unirradiated to the irradiated areas, making the graphene more resistant to the irradiation, and hence leading to smaller pore sizes than expected. This so-called edge effect, however, affects only a small regions of the graphene, about 5 μm from the border. Areas further away from the border are less affected by this effect and feature uniform pore sizes.

Noticeably, in comparison the brightness of the graphene membranes is inversely proportional to the exposed areas: while the 350 nm and the 250 nm membranes are rather dark, and the 15–50 nm membrane is noticeably brighter. Since the brightness in the SEM image is equivalent to the emission yield of secondary electrons, it can also be used to assess qualitatively the cleanliness of the graphene membrane. Lower brightness, i.e. lower emission yield, can be interpreted as thinner, and hence, cleaner graphene. In that sense, the structured graphene with larger pore sizes appears to be cleaner than the graphene with smaller pore sizes. In fact, the SEM image of a graphene membrane outside of the patterning region shows an intact graphene with apparent streaks of contaminants (figure 2(f)). This membrane is also the brightest as compared to other images of figure 2, consistent with the correlation between the brightness of the SEM and the cleanliness of the sample. Furthermore, there is a brighter rectangular in the middle of the image, an area that was intentionally exposed under a reduced scanning window of the electron beam for about 30 s. This observation corresponds well with the well-known build-up of hydrocarbon molecules due to diffusion and accumulation of organic contamination, often occurring in electron microscopy of heavily contaminated samples.

Further information on the cleanliness of the structured graphene can be extracted from data presented in figure 3. The SEM image of figure 3(a) shows the border between the irradiated and the unirradiated regions of the 150 nm pattern. The successfully patterned graphene further away from the borderline (circle 1) appears much darker than the ones outside the pattern (circle 3), similar to observations made from figures 2(c) and (f). Furthermore, within the shown area of the pattern a gradient in brightness is apparent. The area in close proximity to the borderline (circle 2) appears slightly brighter than the one further away from the border (circle 1), although the two areas received exactly the same irradiation. This observation again points towards the argument that excess mobile contaminants diffuse from the other side of the border into the pattern regions. In figures 3(b) and (c), images with higher-resolution for the unirradiated regions (b) and the

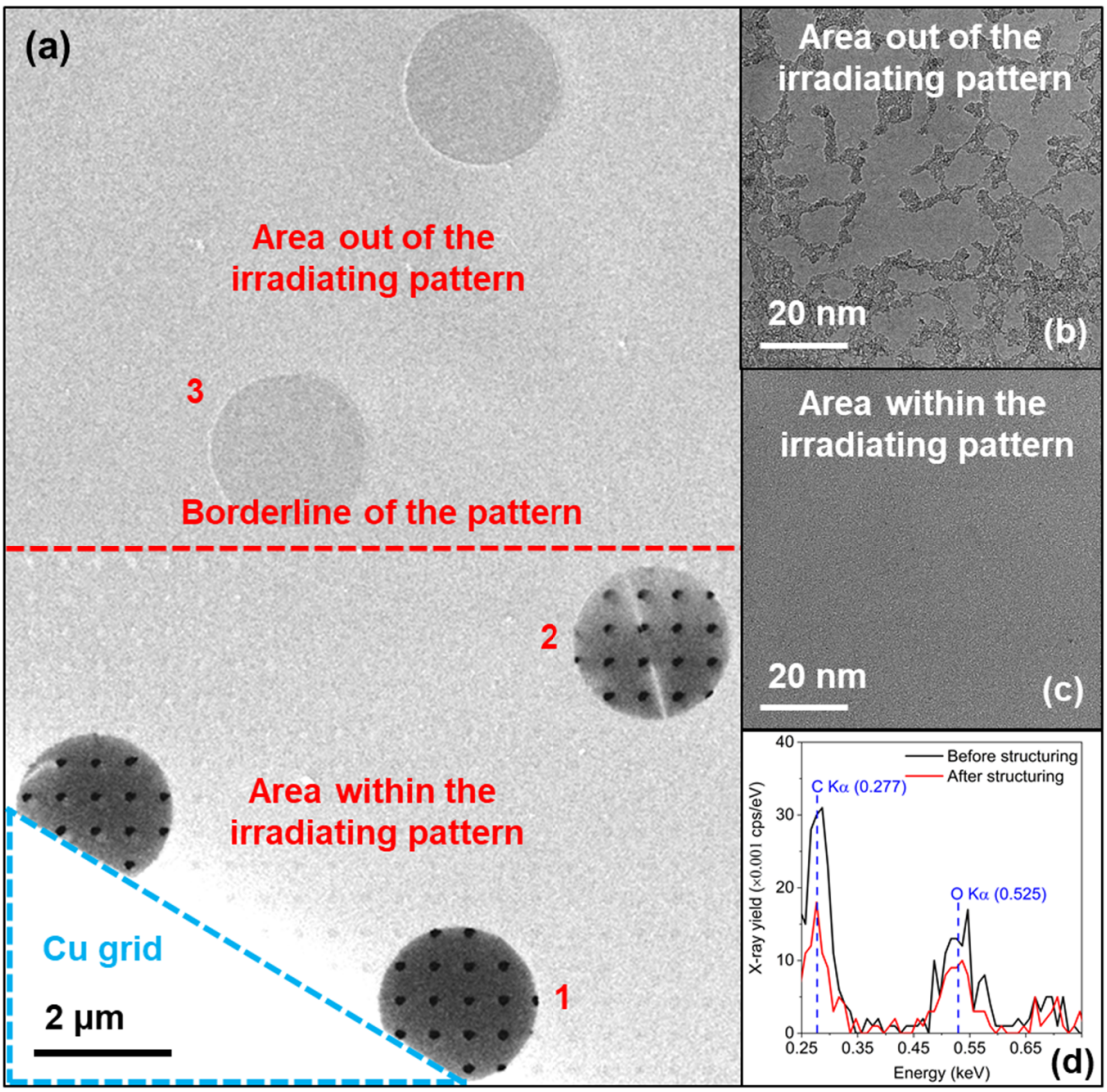

Figure 3. SEM image at lower magnification than the one in figure 2 showing the borderline of the 150 nm pattern (a). Graphene membranes within the irradiation pattern are significantly darker than outside. (b) TEM image of the unirradiated graphene featuring apparent streaks of PMMA contamination. (c) Much cleaner surface and free of streaks are obtained for the unirradiated graphene located within the patterned area. (d) EDX spectra of a region outside (black curve) and a region within the irradiating pattern (red curve).

irradiated region (c) are obtained using bright-field TEM. Imaging in bright-field TEM relies on transmission of electrons through the samples, hence, in contrast to SEM a through-hole pore in the TEM appears brighter and vice versa thicker film appears darker. For areas outside of the irradiating pattern (figure 3(b)), where almost no cleaning effect occurs, the surface of the sample shows a large number of contamination streaks, covering a significant portion of the graphene. For areas within the irradiating pattern, in particular the area around the directly exposed region in figure 3(c) the contamination streaks have been removed to largest extent, i.e. the surface of graphene is smooth, and no streak can be observed. In figure 3(d), we show the energy dispersive x-ray spectroscopy (EDX) data for the sample before (black curve) and after (red curve) the structuring process. The spectra of the sample show only two peaks, C Kα and O Kα, which belongs to the graphene membrane and the hydrocarbon contaminants. These two spectra were recorded for the exactly same area, the same beam current, and the same duration on one sample but at two different regions representing the sample before and after structuring. According to this figure, after structuring the area around the directly irradiated region has lower x-ray yield of carbon and oxygen, which is due to the reduced level of oxygen-containing hydrocarbon contaminants such as PMAA.

Finally, direct evidence showing the diffusion of the mobile contaminants into the exposed areas is shown in figure 4. The bright-field TEM images for an area in proximity to the border of the 110 nm pattern (figure 4(a)) shows periodically arranged black dots, which are interpreted as the accumulation of contamination. According to a calculation using the stopping and range of ion in matters, the nuclear and the electronic energy losses of 20 keV Ar^+ ion in C

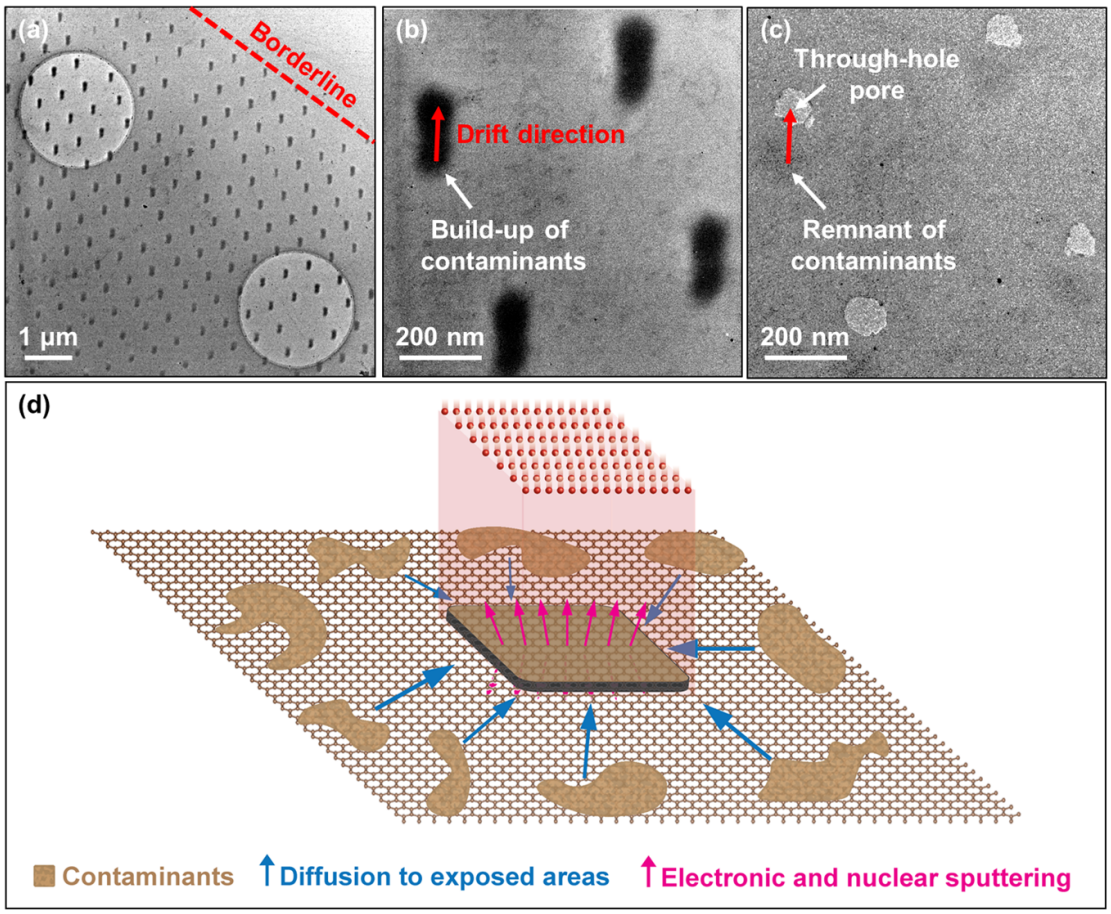

Figure 4. TEM images of the graphene membrane irradiated using the 110 nm pattern (a)–(c) and an illustration of the proposed cleaning mechanism active during the irradiation. The black dots all over the surface in (a) are accumulations of the contaminants under ion beam exposure. These black dots were found in areas close to the border of the pattern, where excessive amounts of contaminants are available. A more magnified image in (b) shows the elongated build-up of contamination due to a slight drift of the mask during the irradiation. Image (c) for the area in proximity to the area of (b), but further away from the border, shows a similar drift (red arrow). One end of the red arrow is the remnant of the contamination build-up, the other end is the through-hole pore.

are 71 and 26 eV/10^{15} At cm^{-2}, respectively. Although the nuclear interactions are dominant, the electronic interactions are also considerable and sufficient to immobilize the diffusing contaminants in the exposed areas, a similar effect as for electron beam exposure shown in figure 2(f). A closer view to this area is given in (b), showing an elongated pattern of the accumulation due to a slight drift of the mask (less than 100 nm) relative to the sample during the irradiation. This drift is less visible in patterns with larger pore sizes due to the higher cleanliness of those patterns. In the area near the one for image (b) but slightly away from the border, through-hole pores were achieved as shown in (c). A similar drift can still be observed in this image with one end of the red arrow showing the remnant of the contamination build-up and the other end showing the through-hole pores.

4. Discussion

In summary, the dynamic behavior of graphene under ion irradiation through the nanopattern mask is illustrated in figure 4(d). Mobile contaminants, normally diffusing in a random manner, are trapped at the exposed areas due to the electronic interactions between the incident ions and the membrane. At the same time, this locally trapped contaminants are subsequently effectively removed by two mechanisms: first, due to the nuclear collisional interactions with the ions, i.e. classical sputtering. Second, in particular weakly-bonded substances might be removed from the material surface due to a slight disturbance in the electronic systems by the electronic energy deposition of the ions striking the surface in their proximity, which is commonly referred to as electronic sputtering. This effect has been reported for fast heavy ions in the orders of MeV. For example, using 1 MeV u^{-1} incident ions, intact large buckyball C_{60} can be ejected from a solid sample of bovine insulin [46]. Medium energy light ions in the orders of keV have been also shown to eject a variety of elemental and organic compound substances from a TiN surface [47]. Although electronic and the nuclear sputtering can both remove the contaminants, the former is much less likely to induce structural damages to the graphene lattice due to the much

stronger covalent bonds in the graphene lattice than the bond between the contaminants and the graphene surface. In the context of preparation of 2DMs, electronic sputtering has not been demonstrated, suggesting a completely new way for cleaning graphene and a vast number of other 2DMs.

The described local accumulation and sputtering of contaminants are two competing processes, and observations presented in this paper can be interpreted in this framework. In figure 4(b), after the irradiation there is still a layer of contaminants accumulated locally on the graphene surface. Although the ablation of the contaminants always occur simultaneously with the accumulation, the rate of ablation is in this case found lower than the rate of accumulation. In contrast, for the area shown in figure 4(c), further away from the border, through-hole pores are achieved because the rate of ablation is higher than the rate of accumulation in this area. The difference in the rate of accumulation between the areas of figures 4(b) and (c) is caused by the amount of contamination surrounding these areas. For the area close to the border of the pattern (figure 4(b)), an excessive amount of contamination is available from the other side of the border which remained unirradiated. These excess contaminants readily diffuse into the exposed area where they accumulate, being locally trapped by the energy deposition of the ions. For the area further away from the border (figure 4(c)), and thus in absence of a large reservoir of contaminants, ablation effectively dominates accumulation. Hence, for chemical vapour deposition (CVD)-grown graphene contamination plays a significant role in the behavior of graphene under ion irradiation as they can form both an effective capping layer preventing the graphene from sputtering, and probably providing carbon atoms for self-healing of the graphene membrane, a process earlier reported in [48].

Revisiting figures 2(d) and (e), these arguments on diffusion of contamination can also explain the modified pore size. The shown area in proximity of the edge of the irradiated area features pores much smaller than the pores of the pattern, from 15–50 nm (figure 2(d)) and 60 nm (figure 2(e)) as compared to 110 nm of the pattern. Again, in these areas, the rate of accumulation is found slightly lower than the rate of sputtering, and hence the perforation process has just started, leading to the decreased pore sizes. In figure 2(e), depicting an area slightly more distant from the border, a larger and more uniform pore size is achieved. Note, that as due to the inwards diffusion, accumulation and self-healing is minimal in the center, which explains, why we observe single perforations smaller than the pores of the mask in the center of the irradiated areas instead of a multitude of smaller holes. In terms of structuring applications, these results suggest that the pore size of the graphene can be tuned to sizes smaller than the pore size of the mask by choosing a proper flux and dose of the irradiation, which is straightforwardly possible with an ion implanter.

5. Conclusions and outlook

In conclusion, a contactless large-area approach for structuring self-supporting graphene at nanoscale has been demonstrated. The structured graphene is shown to have almost identical patterns as determined by the suspended Si mask. The pore sizes of the graphene can also be significantly reduced, down to 15 nm, by utilizing the diffusion effect of the contamination into the exposed areas that makes the graphene more resistant against irradiation. Furthermore, the diffusion of the contamination and its subsequent sputtering gradually exhaust the amount of contamination surrounding the irradiated area and make the overall graphene membrane cleaner. Electronic sputtering of the weakly bound contaminants might also play a role in cleaning of the graphene as it has been reported for other solid materials. Compared to other lithographic methods, which require a masking layer coated directly onto the graphene, leaving it more contaminated, the presented structuring method, additionally can improve the surface quality of the graphene sheets. This simultaneous structuring and cleaning effect has a potential for producing large-area high-quality graphene with customizable nanostructures. We expect that the demonstrated technique can also be employed for creating nanoscale patterns in any other 2DM, such as transitional metal dichalcogenides (TMDCs) and 2D metal carbides/nitrides (MXenes). Since TMDCs and MXenes feature more than one chemical element, preferential sputtering can be expected, probably leading to particular types of defects and hence properties.

Data availability statement

All data that support the findings of this study are included within the article (and any supplementary files).

Acknowledgments

T T thanks Örjan Vallin, staff of Myfab Uppsala, for the very helpful discussion and supports related to the fabrication of the nanopattern mask. T T appreciates technical support from Johan Oscarsson, Sven Cederberg and Mauricio Sortica. We acknowledge Myfab Uppsala for providing facilities and experimental support. Myfab is funded by the Swedish Research Council (2019–00207) as a national research infrastructure. We also acknowledge the Tandem Laboratory, a national infrastructure at Uppsala University, for the access to the ion irradiation experiments.

Author contributions

T T and D P conceptualized and supervised the research. T T, H B and N P conducted experiments. All authors discussed the results and commented on the manuscript. T T wrote the final manuscript. D P and T T acquired funding for the project. The manuscript was written through contributions of all authors. All authors have given approval to the final version of the manuscript.

Funding sources

- The Swedish Research Council VR-RFI (Contracts No. 2017-00646_9 and 2019-00191).
- The Swedish Foundation for Strategic Research (Contract No. RIF14-0053).
- The ÅFORSK FOUNDATION (Ref: 22-313).
- The I BERGHS FOUNDATION.

Conflict of interest

The authors declare no competing financial or non-financial interests.

ORCID iDs

Tuan T Tran https://orcid.org/0000-0002-1393-1723
Daniel Primetzhofer https://orcid.org/0000-0002-5815-3742

References

[1] Bai J, Zhong X, Jiang S, Huang Y and Duan X 2010 Graphene nanomesh *Nat. Nanotechnol.* **5** 190–4
[2] Safron N S, Brewer A S and Arnold M S 2011 Semiconducting two-dimensional graphene nanoconstriction arrays *Small* **7** 492–8
[3] Forsythe C, Zhou X, Watanabe K, Taniguchi T, Pasupathy A, Moon P, Koshino M, Kim P and Dean C R 2018 Band structure engineering of 2D materials using patterned dielectric superlattices *Nat. Nanotechnol.* **13** 566–71
[4] Jessen B S *et al* 2019 Lithographic band structure engineering of graphene *Nat. Nanotechnol.* **14** 340–6
[5] Li G, Zhang S and Zentgraf T 2017 Nonlinear photonic metasurfaces *Nat. Rev. Mater.* **2** 17010
[6] Cox J D and Javier García de Abajo F 2014 Electrically tunable nonlinear plasmonics in graphene nanoislands *Nat. Commun.* **5** 5725
[7] Cox J D and García de Abajo F J 2015 Plasmon-enhanced nonlinear wave mixing in nanostructured graphene *ACS Photon.* **2** 306–12
[8] Sint K, Wang B and Král P 2008 Selective ion passage through functionalized graphene nanopores *J. Am. Chem. Soc.* **130** 16448–9
[9] Jiang D-E, Cooper V R and Dai S 2009 Porous graphene as the ultimate membrane for gas separation *Nano Lett.* **9** 4019–24
[10] Koenig S P, Wang L, Pellegrino J and Bunch J S 2012 Selective molecular sieving through porous graphene *Nat. Nanotechnol.* **7** 728–32
[11] Celebi K, Buchheim J, Wyss R M, Droudian A, Gasser P, Shorubalko I, Kye J-I, Lee C and Park H G 2014 Ultimate permeation across atomically thin porous graphene *Science* **344** 289–92
[12] Nakada K, Fujita M, Dresselhaus G and Dresselhaus M S 1996 Edge state in graphene ribbons: nanometer size effect and edge shape dependence *Phys. Rev.* B **54** 17954–61
[13] Son Y-W, Cohen M L and Louie S G 2006 Energy gaps in graphene nanoribbons *Phys. Rev. Lett.* **97** 216803
[14] Li X, Wang X, Zhang L, Lee S and Dai H 2008 Chemically derived, ultrasmooth graphene nanoribbon semiconductors *Science* **319** 1229–32
[15] Zeng Z, Huang X, Yin Z, Li H, Chen Y, Li H, Zhang Q, Ma J, Boey F and Zhang H 2012 Fabrication of graphene nanomesh by using an anodic aluminum oxide membrane as a template *Adv. Mater.* **24** 4138–42
[16] Wei T, Hauke F and Hirsch A 2021 Evolution of graphene patterning: from dimension regulation to molecular engineering *Adv. Mater.* **33** 2104060
[17] Novoselov K S, Geim A K, Morozov S V, Jiang D, Zhang Y, Dubonos S V, Grigorieva I V and Firsov A A 2004 Electric field effect in atomically thin carbon films *Science* **306** 666–9
[18] Bolotin K I, Sikes K J, Jiang Z, Klima M, Fudenberg G, Hone J, Kim P and Stormer H L 2008 Ultrahigh electron mobility in suspended graphene *Solid State Commun.* **146** 351–5
[19] Cohen-Tanugi D and Grossman J C 2012 Water desalination across nanoporous graphene *Nano Lett.* **12** 3602–8
[20] Surwade S P, Smirnov S N, Vlassiouk I V, Unocic R R, Veith G M, Dai S and Mahurin S M 2015 Water desalination using nanoporous single-layer graphene *Nat. Nanotechnol.* **10** 459–64
[21] Krasheninnikov A V and Nordlund K 2010 Ion and electron irradiation-induced effects in nanostructured materials *J. Appl. Phys.* **107** 071301
[22] Schneider G F, Kowalczyk S W, Calado V E, Pandraud G, Zandbergen H W, Vandersypen L M K and Dekker C 2010 DNA translocation through graphene nanopores *Nano Lett.* **10** 3163–7
[23] Börrnert F, Avdoshenko S M, Bachmatiuk A, Ibrahim I, Büchner B, Cuniberti G and Rümmeli M H 2012 Amorphous carbon under 80 kV electron irradiation: a means to make or break graphene *Adv. Mater.* **24** 5630–5
[24] Buchheim J, Schlichting K-P, Wyss R M and Park H G 2019 Assessing the thickness–permeation paradigm in nanoporous membranes *ACS Nano* **13** 134–42
[25] Bae S *et al* 2010 Roll-to-roll production of 30-inch graphene films for transparent electrodes *Nat. Nanotechnol.* **5** 574–8
[26] Yang Y, Yang X, Liang L, Gao Y, Cheng H, Li X, Zou M, Ma R, Yuan Q and Duan X 2019 Large-area graphene-nanomesh/carbon-nanotube hybrid membranes for ionic and molecular nanofiltration *Science* **364** 1057–62
[27] Madauß L, Ochedowski O, Lebius H, Ban-d'Etat B, Naylor C H, Johnson A T C, Kotakoski J and Schleberger M 2016 Defect engineering of single- and few-layer MoS_2 by swift heavy ion irradiation *2D Mater.* **4** 015034
[28] Kozubek R *et al* 2019 Perforating freestanding molybdenum disulfide monolayers with highly charged ions *J. Phys. Chem. Lett.* **10** 904–10
[29] Creutzburg S *et al* 2021 Fluorination of graphene leads to susceptibility for nanopore formation by highly charged ion impact *Phys. Rev. Mater.* **5** 074007
[30] Grossek A S, Niggas A, Wilhelm R A, Aumayr F and Lemell C 2022 Model for nanopore formation in two-dimensional materials by impact of highly charged ions *Nano Lett.* **22** 9679–84
[31] Ghorbani-Asl M, Kretschmer S and Krasheninnikov A V 2022 *Defects in Two-Dimensional Materials* ed R Addou and L Colombo (Amsterdam: Elsevier) pp 259–301
[32] Kim M, Safron N S, Han E, Arnold M S and Gopalan P 2010 Fabrication and characterization of large-area, semiconducting nanoperforated graphene materials *Nano Lett.* **10** 1125–31

[33] Cagliani A, Mackenzie D M A, Tschammer L K, Pizzocchero F, Almdal K and Bøggild P 2014 Large-area nanopatterned graphene for ultrasensitive gas sensing *Nano Res.* **7** 743–54
[34] Mackenzie D M A, Smistrup K, Whelan P R, Luo B, Shivayogimath A, Nielsen T, Petersen D H, Messina S A and Bøggild P 2017 Batch fabrication of nanopatterned graphene devices via nanoimprint lithography *Appl. Phys. Lett.* **111** 193103
[35] Gopalan K K, Paulillo B, Mackenzie D M A, Rodrigo D, Bareza N, Whelan P R, Shivayogimath A and Pruneri V 2018 Scalable and tunable periodic graphene nanohole arrays for mid-infrared plasmonics *Nano Lett.* **18** 5913–8
[36] Gowthami T, Kurra N and Raina G 2014 Interaction and dynamics of ambient water adlayers on graphite probed using AFM voltage nanolithography and electrostatic force microscopy *Nanotechnology* **25** 155304
[37] Gowthami T, Tamilselvi G, Jacob G and Raina G 2015 The role of ambient ice-like water adlayers formed at the interfaces of graphene on hydrophobic and hydrophilic substrates probed using scanning probe microscopy *Phys. Chem. Chem. Phys.* **17** 13964–72
[38] Giesbers A J M, Peters E C, Burghard M and Kern K 2012 Charge transport gap in graphene antidot lattices *Phys. Rev.* B **86** 045445
[39] Winter A, Ekinci Y, Gölzhäuser A and Turchanin A 2019 Freestanding carbon nanomembranes and graphene monolayers nanopatterned via EUV interference lithography *2D Mater.* **6** 021002
[40] Lin Y-C, Lu C-C, Yeh C-H, Jin C, Suenaga K and Chiu P-W 2012 Graphene annealing: how clean can it be? *Nano Lett.* **12** 414–9
[41] Tripathi M, Mittelberger A, Mustonen K, Mangler C, Kotakoski J, Meyer J C and Susi T 2017 Cleaning graphene: comparing heat treatments in air and in vacuum *Phys. Status Solidi* **11** 1700124
[42] Pettes M T, Jo I, Yao Z and Shi L 2011 Influence of polymeric residue on the thermal conductivity of suspended bilayer graphene *Nano Lett.* **11** 1195–200
[43] Lin L *et al* 2019 Towards super-clean graphene *Nat. Commun.* **10** 1912
[44] Zhuang B, Li S, Li S and Yin J 2021 Ways to eliminate PMMA residues on graphene—superclean graphene *Carbon* **173** 609–36
[45] Yang X and Yan M 2020 Removing contaminants from transferred CVD graphene *Nano Res.* **13** 599–610
[46] Johnson R E and Sundqvist B U R 1992 Electronic sputtering: from atomic physics to continuum mechanics *Phys. Today* **45** 28–36
[47] Lohmann S and Primetzhofer D 2018 Ion-induced particle desorption in time-of-flight medium energy ion scattering *Nucl. Instrum. Methods Phys. Res.* B **423** 22–26
[48] Zan R, Ramasse Q M, Bangert U and Novoselov K S 2012 Graphene reknits its holes *Nano Lett.* **12** 3936–40